

In-medium bound states of two bosonic impurities in a one-dimensional Fermi gas

D. Huber,^{1,*} H.-W. Hammer,^{1,2,†} and A. G. Volosniev^{1,3,‡}

¹*Institut für Kernphysik, Technische Universität Darmstadt, 64289 Darmstadt, Germany*

²*ExtreMe Matter Institute EMMI, GSI Helmholtzzentrum für Schwerionenforschung, 64291 Darmstadt, Germany*

³*Institute of Science and Technology Austria, Am Campus 1, 3400 Klosterneuburg, Austria*

(Dated: August 8, 2019)

We investigate the ground-state energy of a one-dimensional Fermi gas with two bosonic impurities. First, we consider the case where impurity and gas atoms have equal masses. The impurity-impurity two-body interaction is identical to the atom-impurity interaction, such that the system is solvable with the Bethe ansatz. We find that the energy of the impurity-impurity subsystem is below that in free space, which we interpret as a manifestation of attractive interactions induced by the Fermi gas. Second, we construct an effective model to describe these interactions, and compare its predictions to the exact solution. We use this effective model to study non-integrable systems with unequal masses and/or potentials.

I. INTRODUCTION

An environment with mobile impurity atoms is a cherished model system in quantum physics. It is a testbed for introducing and testing quasiparticle concepts, e.g., polarons and bipolarons, which naturally appear when studying the movement of electrons in crystals [1–3], ³He atoms in superfluid ⁴He [4], or even protons in neutron matter [5]. Nowadays, these concepts can be examined using ultracold atoms [6–11] – state-of-the-art quantum analog computers. An important topic that can be addressed with cold atom systems is the physics of impurity-impurity interactions induced by a medium [12–22]. This topic is relevant for basic research, and in applications motivated by bound states of dressed electrons and their relation to high- T_c superconductors [23],[24].

In this paper, we calculate the ground-state energy of a one-dimensional (1D) Fermi gas with two bosonic impurities, see Fig. 1. One-dimensional geometries typically enhance interaction effects [25] opening up the possibility of observing bound states supported by the induced attraction [26]. Another feature that separates one spatial dimension from higher dimensions is the long-range tail of correlations. For example, Friedel oscillations [27] decay as $\sim 1/r^D$ where D is the dimension of space. These enhanced correlations may be useful to simulate phenomena beyond short-range physics typical for cold atoms.

Our paper is organized as follows. We start by introducing the Hamiltonian of our 1D model in Section II. In Section III, we study impurity-impurity correlations in the limiting case of equal masses, $M = m$. All interactions are identical and parametrized by Dirac delta functions. The fermions do not interact among each other due to the Pauli exclusion principle. The system is solvable by the Bethe ansatz, which is a common start-

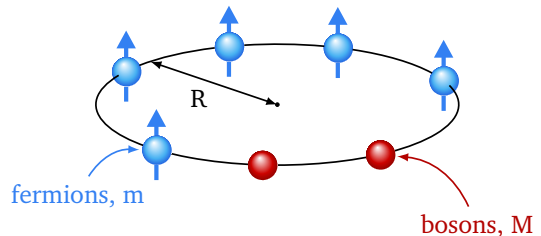


Figure 1. An illustration of the system: Two bosonic impurities in a one-dimensional Fermi gas. Periodic boundary conditions are employed, i.e., the system lives on a ring of radius R . The mass of an impurity (fermion) is denoted M (m).

ing point for analyzing cold atom systems in 1D geometries [28–30]. In Section IV, we go on to discuss effective models for describing two impurities in a medium and benchmark them against the Bethe ansatz results. Afterwards, we use the models to investigate non-integrable systems; our focus is on the appearance of in-medium bound states. The transition from unbound impurities to bound impurities can be tested in cold atom experiments, for example, by measuring the spectroscopic response or by studying the collapse dynamics [22] in imbalanced Bose-Fermi mixtures. Finally, Section V contains a summary of our results and an outlook.

II. FORMULATION

We consider two bosonic impurities interacting via a zero-range potential with N_f spinless (fully spin-polarized) fermions. For convenience, we assume that N_f is an odd number. This assumption does not limit the generality of our results as we are interested in the limit $N_f \rightarrow \infty$. The particles are confined to a ring of radius R , see Fig. 1. The Hamiltonian for the system reads

$$H = H_f + H_b + V_{fb}, \quad (1)$$

* dhuber@theorie.i.kp.physik.tu-darmstadt.de

† hammer@theorie.i.kp.physik.tu-darmstadt.de

‡ volosniev@theorie.i.kp.physik.tu-darmstadt.de

where H_f describes fermions:

$$H_f = - \sum_{j=1}^{N_f} \frac{\hbar^2}{2m} \frac{\partial^2}{\partial X_j^2}, \quad (2)$$

with m the fermion mass. H_b describes the impurity bosons:

$$H_b = - \frac{\hbar^2}{2M} \frac{\partial^2}{\partial Y_1^2} - \frac{\hbar^2}{2M} \frac{\partial^2}{\partial Y_2^2} + g_{II} \delta(Y_1 - Y_2), \quad (3)$$

where M is the boson mass, and g_{II} is the strength of the boson-boson interaction. The interaction between fermions and bosons is written as

$$V_{fb} = g \sum_{i,j} \delta(Y_i - X_j), \quad i = 1, 2; j = 1, \dots, N_f, \quad (4)$$

where g is the corresponding interaction strength. We solve the Schrödinger equation $H\psi = \epsilon\psi$ for the ground state for different N_f and sizes $L = 2\pi R$ of the system. Then, we extrapolate the energies to the thermodynamic limit, $N_f, L \rightarrow \infty$, assuming a fixed density of the Fermi gas, $N_f/L = \rho$. For convenience, we introduce the dimensionless quantities $y_j = Y_j\rho$, $x_j = X_j\rho$, $l = L\rho$, $c_{II} = mg_{II}/(\hbar^2\rho)$, $c = mg/(\hbar^2\rho)$, and $\epsilon = 2m\epsilon/(\hbar^2\rho^2)$.

III. SOLVABLE LIMITS

A. Bethe-Ansatz-Solvable Case

First, we consider the most symmetric case: $c_{II} = c$ and $m = M$, whose Hamiltonian we write as

$$h_{BA} = - \sum_{j=1}^N \frac{\partial^2}{\partial x_j^2} + 2c \sum_{j<l}^N \delta(x_j - x_l), \quad (5)$$

where we set $x_{N-1} = y_1$ and $x_N = y_2$ to explicitly demonstrate the particle exchange symmetry. The ground state of h_{BA} with fermions at the coordinates (x_1, \dots, x_{N_f}) and bosons at (x_{N-1}, x_N) can be studied experimentally with SU(3)-symmetric fermions, e.g., with ^{173}Yb [31]. Indeed, the ground state of SU(3) fermions with the particle decomposition $N_f + 1 + 1$ has a bosonic symmetry for the exchange of the two spin deviates. To understand this, note that: i) the two spin deviates are distinguishable particles and, hence, there exist no a priori symmetry requirements for their exchange; ii) the Hamiltonian h_{BA} commutes with the particle exchange operator; iii) the bosonic symmetry leads to the lowest energy.

The spectrum of the Hamiltonian h_{BA} can be found using the Bethe ansatz (BA) [32]. For every ordering of particles (e.g., for $x_1 < x_2 < \dots < x_N$), the wave function is written as a sum of the plane waves $e^{i\sum_j k_j x_j}$. For this wave function to fulfill the boundary conditions at $x_i = 0$, $x_i = l$ and $x_i = x_j$ for all i and j , the wave vectors k_j

must satisfy the BA equations

$$e^{ik_j l} = \frac{k_j - \Lambda_1 + \frac{ic}{2}}{k_j - \Lambda_1 - \frac{ic}{2}} \frac{k_j - \Lambda_2 + \frac{ic}{2}}{k_j - \Lambda_2 - \frac{ic}{2}}, \quad 1 \leq j \leq N; \quad (6)$$

$$\prod_{j=1}^N \frac{k_j - \Lambda_1 + \frac{ic}{2}}{k_j - \Lambda_1 - \frac{ic}{2}} = 1, \quad \prod_{j=1}^N \frac{k_j - \Lambda_2 + \frac{ic}{2}}{k_j - \Lambda_2 - \frac{ic}{2}} = 1;$$

where the bosonic and fermionic symmetries have already been implemented [33–35]. Λ_1 and Λ_2 are to be determined together with the set $\{k_j\}$. Once the BA equations are solved, the energy of the system is determined as $\epsilon = \sum_{j=1}^N k_j^2$. Note that the number of unknowns in Eqs. (6) for the ground state can be reduced to $(N_f+3)/2$ from N_f+4 . Indeed, the total (angular) momentum must be zero in the ground state, $\sum_j k_j = 0$. This together with the fact that the wave function is real makes the wave vectors appear in pairs (we exemplify this below). In addition, one can show that $\Lambda_1 = -\Lambda_2$.

To solve Eq. (6) for the ground state, we apply Newton's method, which requires an accurate initial estimate of k_j and Λ_j . For $c \rightarrow 0$, we obtain this estimate directly from the BA equations (see Appendix A):

$$k_1 \simeq \sqrt{\frac{3c}{l}}, \quad k_2 \simeq -\sqrt{\frac{3c}{l}}, \quad k_3 \simeq 0,$$

$$k_j \simeq k_j^{(0)} + \frac{2c}{k_j^{(0)} l}, \quad \text{for } 4 \leq j \leq N; \quad (7)$$

$$\Lambda_1 \simeq \sqrt{\frac{c}{l}}, \quad \Lambda_2 \simeq -\sqrt{\frac{c}{l}},$$

where $k_j^{(0)}$ is the wave vector at $c = 0$. Note that in Eq. (7) the wave vectors are related pairwise, e.g., $k_1 = -k_2$, as has already been mentioned. The only non-paired wave vector is $k_3 = 0$. Estimate (7) allows us to calculate $\{k_i\}$ for weak interactions. An initial guess for moderate interactions is obtained from a Taylor series constructed using solutions at smaller values of c .

We solve Eq. (6) for a sequence of N_f and extrapolate to the thermodynamic limit. To this end, we subtract from the energy the zero-interaction offset and fit the difference with $\epsilon(c) - \epsilon(0) = \epsilon_\infty + A_1/N + A_2/N^2$, where ϵ_∞, A_1 and A_2 are fitting parameters. It is straightforward to argue for the form of the fitting function, $\epsilon_\infty + A_1/N + A_2/N^2$, in the case of strong interactions ($c \rightarrow \pm\infty$) for which the energies can be calculated using a non-interacting Fermi gas. We do not attempt to validate the fitting function for finite values of c , since we observe that the form of the function is not important for our analysis (see Appendix B).

To investigate induced correlations, we introduce the ‘‘in-medium binding energy’’ $E = \epsilon_\infty - 2\mathcal{E}$, where \mathcal{E} is the energy gain for immersing one impurity in a Fermi gas [36, 37] (see Appendix C). The quantity $2\mathcal{E}$ describes the energy of two non-correlated impurities. E is presented in Fig. 2. We say that if $E = 0$ there is no in-medium bound state, whereas if $E < 0$ then there is at least one. Next, we analyze cases with $c < 0$ and $c > 0$

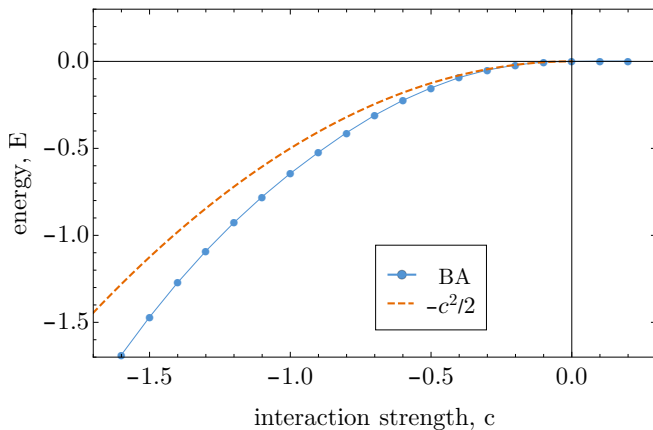


Figure 2. The (blue) dots show the in-medium binding energy of two bosonic impurities in a Fermi gas for the Bethe-ansatz-integrable case, the size of the dots can be used as an error estimate. The solid (blue) curve is added to guide the eye. The dashed (orange) curve shows the binding energy of two bosons in free space. We interpret the gap between the solid and the dashed curves as a manifestation of attractive impurity-impurity interactions mediated by the Fermi gas.

separately.

Repulsive interactions, $c > 0$. We calculate the energy for $c \lesssim 2$ and find that $E = 0$ (within numerical accuracy), which means that there are no in-medium bound states. For $c \rightarrow 0$ this can be understood, since the impurity-impurity interaction in free space scales as c (see Eqs. (3) and (5)), whereas the induced impurity-impurity interaction is expected to scale as c^2 (see Sec. IV). Therefore, the interaction volume, i.e., the space integral of the effective impurity-impurity interaction, is necessarily a small positive quantity for $c \rightarrow 0$, which does not allow for the existence of a bound state [38, 39].

In the limit of strong interactions some extra insight can also be gained. For $c \rightarrow \infty$ the important degrees of freedom are spins [40–43], which allows one to map the Hamiltonian h_{BA} onto an XX spin chain [44] with constant coefficients,

$$h_{BA} \rightarrow -\frac{J}{2} \sum (\sigma_x^i \sigma_x^{i+1} + \sigma_y^i \sigma_y^{i+1}), \quad (8)$$

where σ_x^i and σ_y^i are the Pauli matrices acting on the spin at site i ; J is an exchange coefficient proportional to $1/c$, see [45] for the derivation in a homogeneous environment. The system in Fig. 1 with $c \rightarrow \infty$ is then identical to a linear spin chain with two spin deviates (magnons) for which a bound state is not expected [46].

Attractive interactions, $c < 0$. Figure 2 shows that for $c < 0$ there is an in-medium bound state whose energy is below the ground state energy of the Hamiltonian that describes two bosons without the Fermi gas, i.e., H_b from Eq. (3). This lowering of the energy is a manifestation of the induced impurity-impurity correlations, which we interpret in Sec. IV using an effective impurity-impurity

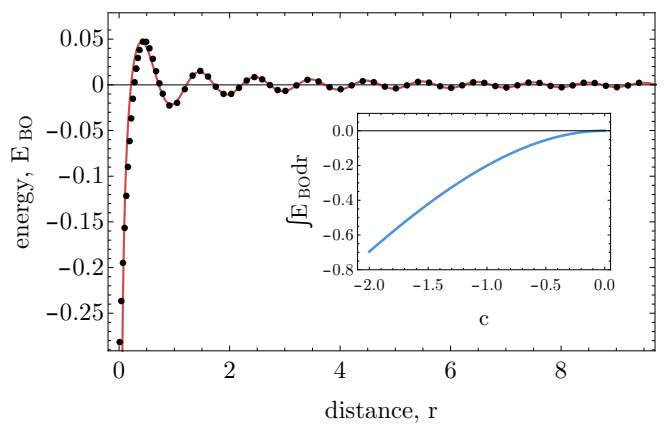


Figure 3. The energy of a Fermi gas with two static impurities. The dots show our results for $c = -0.5$. The curve shows the fit to the long-range tail [47, 48] $B \cos(Ar + \delta)/r$ for $c \rightarrow 0$, where A, B and δ are fitting parameters. Note that the fit is accurate almost everywhere, except the region of $r \rightarrow 0$, where the exact result must be used. The inset present the integral of E_{BO} over the entire space.

potential. Since we are interested in interactions mediated by the Fermi gas, we do not discuss in this paper the limit $c \rightarrow -\infty$, which implies the formation of a tightly bound few-body state. We only explore $c \gtrsim -2$.

B. Two Static Impurities

Before we discuss effective models that describe two mobile impurities in a sea of fermions, we consider two static impurities $M \rightarrow \infty$ – another analytically solvable limit of the Hamiltonian (1). The solution is obtained by solving the one-body problem: one particle in a ring with a potential due to the two impurities fixed at $-r/2$ and $r/2$

$$h_{BO} = -\frac{\partial^2}{\partial x^2} + 2c \left[\delta \left(x - \frac{r}{2} \right) + \delta \left(x + \frac{r}{2} \right) \right], \quad (9)$$

where the subscript emphasizes the connection to the Born-Oppenheimer (BO) approximation, which will be employed below. The spectrum of h_{BO} depends on the distance r . We calculate this dependence only for attractive interactions, i.e., $c < 0$; the repulsive case can be calculated in a similar manner. To obtain the ground state energy of the Fermi gas, $\varepsilon_{BO}(c, r)$, we add the energies of the lowest N_f eigenstates of the Hamiltonian h_{BO} (see Appendix D). The thermodynamic limit is calculated by extrapolating the results for systems with different values of N_f and l and a fixed ratio N_f/l . We observe that already for $N_f = 19$ the energy for small values of r reproduces accurately the energy in the thermodynamic limit. The solution for larger values of r is obtained by fitting to the known form of the tail [47, 48].

Figure 3 illustrates the energy $E_{BO}(r) = \varepsilon_{BO}(c, r) - \varepsilon_{BO}(0, r) - 2\mathcal{E}_{static}$ for $c = -0.5$ (we assume that $g_{II} = 0$

for the sake of discussion). \mathcal{E}_{static} is the energy gain for immersing a single static impurity in a Fermi gas [49]

$$\mathcal{E}_{static}(c) = \left(\pi + \frac{c^2}{\pi}\right) \arctan\left(\frac{c}{\pi}\right) + c - \frac{c^2}{2}. \quad (10)$$

The quantity E_{BO} has a deep minimum at $r = 0$ given by $\mathcal{E}_{static}(2c) - 2\mathcal{E}_{static}(c)$ and an oscillatory tail. For $c \rightarrow 0$ the tail can be written simply as $c^2 \cos(Ar + \delta)/r$, where A and δ are constants. The form of the tail in this limit can be related to Friedel oscillations [27]. These oscillations determine the density of the Fermi gas at the position of the second impurity, provided that the first impurity is separated by the distance r . This density in turn determines the energy of the system, according to first order perturbation theory. It is worthwhile noting that the dependence of E_{BO} on r is observable. It can, in principle, be probed in cold atom experiments by spectroscopy [47].

IV. EFFECTIVE MODEL

A. Bethe-ansatz-solvable system

The ground state of a one-dimensional Fermi gas with a single impurity is orthogonal to the ground state of the corresponding non-interacting system. This phenomenon is related to the Anderson orthogonality catastrophe [50]. For the SU(2) symmetric case it can be conveniently studied using the BA equations [51]. This orthogonality reduces the applicability of the polaron picture. For example, the dynamics after a sudden change of parameters cannot be captured by a single quasiparticle, instead it requires a continuum of states. Still, the notion of the effective mass and self-energy can be used to describe the low-energy spectrum of a Fermi gas with one impurity [36, 37, 51–53], suggesting the use of the following Hamiltonian to model the binding energy for the system of two impurities

$$h_{\text{eff}} = -\frac{m}{m_{\text{eff}}} \frac{\partial^2}{\partial y_1^2} - \frac{m}{m_{\text{eff}}} \frac{\partial^2}{\partial y_2^2} + W(y_1 - y_2), \quad (11)$$

where $m_{\text{eff}}(c)$ is the effective mass of the impurity [37, 51, 52], so that the Hamiltonian h_{eff} with $W = 0$ correctly describes the low-energy spectrum of two non-interacting impurities. For attractive interactions considered here, $c \in (-2, 0)$, the effective mass can be written as

$$\frac{m_{\text{eff}}}{m} \simeq 1 + \frac{c^2}{\pi^4} + \left(\frac{2}{\pi^6} - \frac{1}{6\pi^4}\right) c^3 + \left(\frac{4}{\pi^8} - \frac{1}{2\pi^6}\right) c^4. \quad (12)$$

This equation shows that the mass does not increase by more than a few percent for the considered parameters.

The function W in Eq. (11) describes the impurity-impurity correlations. We write it as

$$W(y_1 - y_2) = 2c\delta(y_1 - y_2) + V(y_1 - y_2), \quad (13)$$

where the first term is the interaction between impurities

in free space; the second term is an effective interaction mediated by the environment. Note that the exact shape of V is not required. We are interested in the weak and moderate interaction regimes for which the knowledge of a few integrated properties of V is sufficient, e.g., only $\int V(y)dy$ determines the binding energy for $c \rightarrow 0$. Indeed, the ground state energy E_{eff} of h_{eff} for weak interactions reads [38, 39]

$$E_{\text{eff}} \simeq -\frac{m_{\text{eff}}}{8m} \left[\int_{-\infty}^{\infty} W(y)dy \right]^2, \quad (14)$$

which can be expanded as

$$E_{\text{eff}} = -\frac{c^2}{2} - \frac{c}{2} \int V(y)dy + O(c^4), \quad (15)$$

where we assume that $\int Vdy$ scales as c^2 (see below) to estimate the neglected pieces. Note that the renormalization of mass enters in $O(c^4)$ meaning that this effect may be disregarded for $c \rightarrow 0$ when compared to the effect of the two-body effective interaction. The first term in Eq. (15) is the ground state energy of two particles in free space. The integral $\int Vdy$ must be negative to ensure that the energy of the in-medium bound state is below $-c^2/2$ as in Fig. 2. Therefore, the effective interaction must be overall attractive. Let us discuss the two (arguably) simplest approximations that can be used to calculate V .

Zero-range Potential. The most basic form of V in Eq. (13) consistent with the first two terms of the expansion (15) is the zero-range (ZR) potential

$$V_{ZR}(y_1 - y_2) = -\kappa\delta(y_1 - y_2), \quad (16)$$

where $\kappa \equiv |\int Vdy|$. This potential can be used to reproduce low-energy properties of two impurities when higher order terms in Eq. (15) are not important. The parameter κ can be obtained, for example, from a single-phonon exchange [13], in which case $\kappa = 2c^2/\pi^2 \simeq 0.202c^2$ for $c \rightarrow 0$. If the potential

$$W_{ZR}(y_1 - y_2) = [2c - 2c^2/\pi^2] \delta(y_1 - y_2) \quad (17)$$

is used in Eq. (11) then a single bound state with the energy

$$E_{\text{eff}}^{ZR} = -\frac{m_{\text{eff}}}{2m} (c - c^2/\pi^2)^2 \quad (18)$$

is produced. This effective model captures qualitatively the exact results, see Fig. 4 (top). We show the ground state energies of h_{eff} with m_{eff} from Eq. (12) and with $m_{\text{eff}} = m$, to illustrate that the mass renormalization leads only to a marginal correction for the considered values of c .

Induced interaction from the Born-Oppenheimer approximation. The potential V in Eq. (13) can also be derived in the Born-Oppenheimer approximation, where it is assumed that the Fermi gas follows the impurity adiabatically. The potential in this case is simply the energy in Fig. 3. This approximation must be accurate if the impurity is very heavy. For mobile impurities this

approximation is accurate if the impurities move slowly in comparison to the Fermi velocity, which defines the dispersion of a sound mode in a Fermi gas.

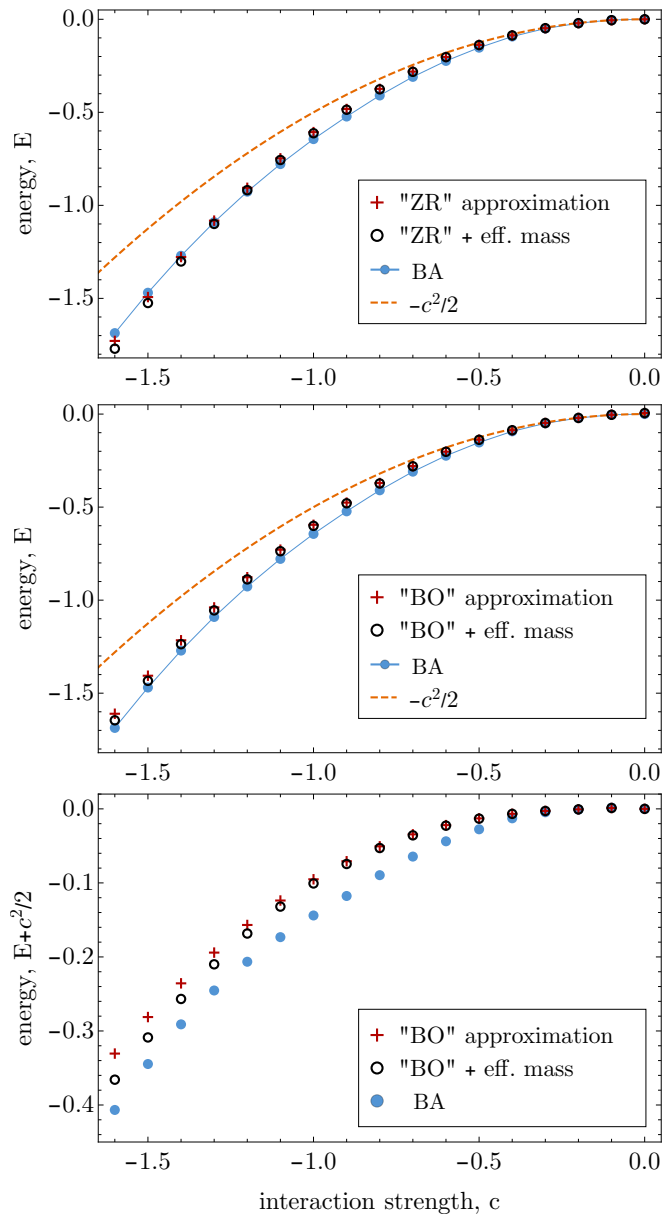


Figure 4. The in-medium binding energy of two impurities in a Fermi gas compared to the zero-range and Born-Oppenheimer approximations. The dots show the exact BA results as in Fig. 2, while the dashed curve shows the binding energy of two bosons in free space. Top: Comparison to the zero-range approximation, Eq. (18), with m_{eff} from Eq. (12) (circles) and the result for $m_{\text{eff}} = m$ (crosses). Center: Comparison to the Born-Oppenheimer approximation with the potential from Fig. 3 and m_{eff} from Eq. (12) (circles) and the result for $m_{\text{eff}} = m$ (crosses). Bottom: The data from the center panel shifted by $c^2/2$ and displayed on a larger scale.

The function $E_{BO}(y_1 - y_2)$ decays as $1/|y_1 - y_2|$, however, it leads to an effectively short-range potential due

to the oscillatory tail. For example, $\int E_{BO}(y)dy$ is well-defined. We calculate that $|\int E_{BO}(y)dy| \simeq 0.22c^2$ for $c \rightarrow 0$. This is slightly larger than $\kappa \simeq 0.202c^2$ for the zero-range potential discussed above. Even though, the long-range tail is not expected for integrable systems [13], the potential E_{BO} performs as well as the zero-range potential, confirming that only integral properties of V are important. Figure 4 (center) gives the binding energy calculated using the potential

$$W_{BO} = 2c\delta(y_1 - y_2) + E_{BO}(y_1 - y_2). \quad (19)$$

Figure 4 (bottom) shows the quantity $E + c^2/2$ to single out the effect of the induced interaction. The center and bottom panels of Fig. 4 demonstrate that the E_{BO} can be used to qualitatively analyze in-medium bound states. To reduce the disagreement between the exact results and the effective model in Fig. 4 (bottom) one can include couplings between eigenstates of h_{BO} due to the motion of the impurities. We leave this discussion for future studies.

To calculate the data in Fig. 4 (center, bottom), we exactly diagonalize the Hamiltonian h_{eff} : We use the eigenstates of the effective Hamiltonian with $W = 0$ as a basis to write h_{eff} as a matrix and diagonalize this matrix after truncation. The energy is found by fitting to the form $E_K = E_{\text{eff}} + D/K$, where K is the number of used basis states and D, E_{eff} are fitting parameters. This slow $1/K$ -convergence is expected for zero-range interactions [54].

Other potentials. The effective potential can also be calculated using other approximation schemes. For example, trial wave functions [16, 55, 56] can be used. We do not discuss those approaches here. However, we note that different methods may lead to different shapes of the effective potential. This is not surprising, since the effective potential is not an observable quantity for mobile impurities.

B. Non-integrable cases

Motivated by the accuracy of the effective model (11) for the most symmetric case, we extend this model to study appearance of in-medium bound states in non-integrable systems, i.e., $c_{II} \neq c$ and/or $m \neq M$. We write the corresponding effective Hamiltonian as

$$h_{\text{eff}} = -\frac{m}{M} \frac{\partial^2}{\partial y_1^2} - \frac{m}{M} \frac{\partial^2}{\partial y_2^2} + 2c_{II}\delta(y_1 - y_2) + V(y_1 - y_2), \quad (20)$$

where we use $m_{\text{eff}} = M$ for simplicity. This approximation relies on the observation that the mass renormalization is not important for the Bethe-ansatz-integrable case for weak interactions. h_{eff} supports a bound state for all $c_{II} < 0$ because the induced interaction is attractive. For $c_{II} > 0$ the bound states appear only if $c_{II} < c_{II}^{\text{cr}}$ for which the repulsive impurity-impurity interaction in free space is overtaken by the attractive interaction mediated by the Fermi gas.

We first consider the case when $c_{II} \neq c$ and $m = M$, in which the particle exchange symmetry is broken by the interaction term [57]. The kinetic energy is still symmetric with respect to the exchange of two particles. We calculate binding energies using the zero-range effective potential and the potential from the adiabatic approximation, see Fig. 5 (top). Both potentials lead to similar results for $c_{II} = 0$ and small values of c , where the one-phonon exchange potential works well. For larger values of c the ZR potential must be corrected.

For $c_{II} = 0.2$ the ZR potential predicts that the in-medium bound state is formed at smaller values of c in comparison to the BO potential, see Fig. 5 (top). The difference between c_{II}^{cr} in the two methods is, however, marginal and one can use the ZR potential to derive the critical value for the appearance of the bound state

$$c_{II}^{cr} \simeq \frac{c^2}{\pi^2}. \quad (21)$$

The transition from an overall repulsive to an overall attractive induced interaction can potentially be studied in Bose-Fermi mixtures by looking, for example, at the collapse dynamics [22]: a Bose gas can be stable only if its particles repel each other. One could also study spectroscopically the energy needed to break a bound state by transferring the system into a non-interacting state. Let us estimate the in-medium binding energy for $m = M$. For $c = -2$ and $c_{II} = 0$, we have $E \simeq -0.06$ (see Fig. 5 (center)), which for ${}^6\text{Li}$ atoms with $\rho = 3/(\mu m)$ translates into $\simeq 22k_B \times nK$, where k_B is the Boltzmann constant. This means that in-medium bound states can be formed only at ultracold temperatures.

The in-medium binding energy can be increased if the impurities are heavy, cf. Eq. (14). To explicitly show this, we consider $c_{II} \neq c$ and $m \neq M$. In this case both the interaction and kinetic energies are not symmetric with respect to the exchange of two particles. For the sake of discussion, we first use the BO potential to calculate the energies of the system with $M = 2m$, see Fig. 5 (center). The behavior of the energy resembles that for $m = M$, but, as expected, the overall energy scale is now larger. It is worthwhile noting that the critical value c_{II}^{cr} obtained using the ZR approximation does not depend on the mass M . A similar conclusion is reached also for the BO potential. Therefore, Eq. (21) can be used to predict the appearance of bound states for different masses of the impurity.

Finally, we consider two bosonic ${}^{133}\text{Cs}$ atoms in a fermionic gas of ${}^6\text{Li}$ as in the experiment of Ref. [22], see Fig. 5 (bottom). We use both the Born-Oppenheimer potential as well as the zero-range potential. Note however that for $M \gg m$ the former is expected to perform better than the latter. For a Li-Cs mixture the energy scale is larger than that for lighter impurities and the bound states should be observable at much higher temperatures.

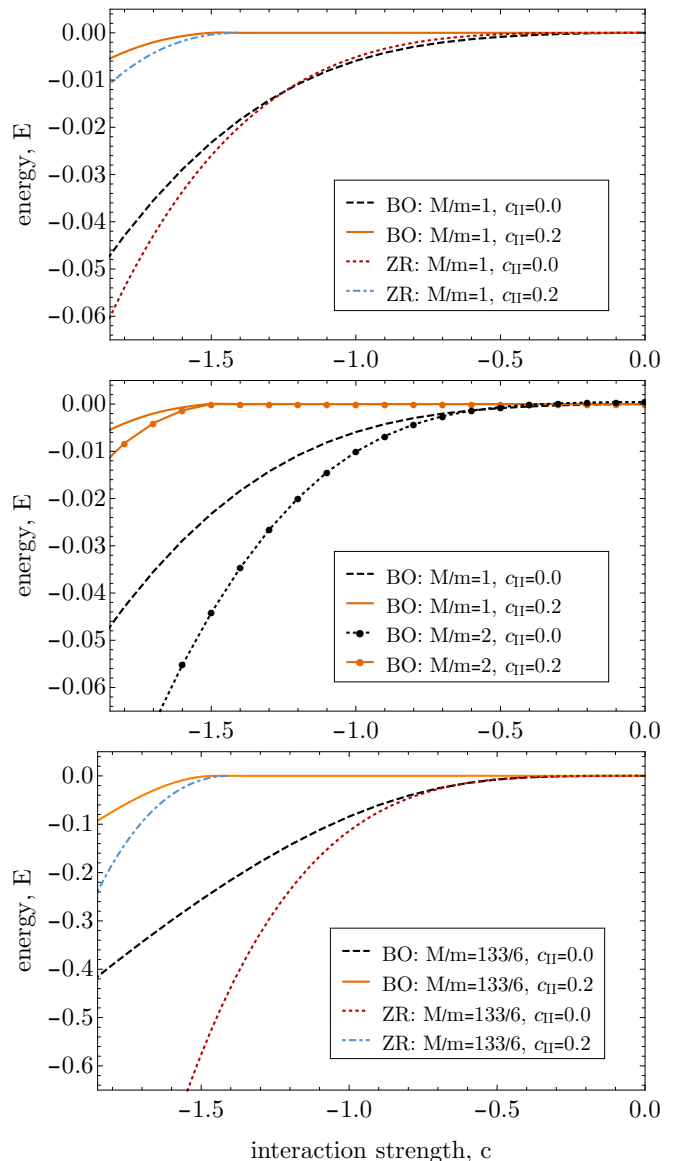


Figure 5. The ground-state energy for two impurities in a Fermi gas in non-integrable cases. We show results for the effective Hamiltonian h_{eff} with $m_{\text{eff}} = M$ for the BO potential from Fig. 3 and the ZR approximation in Eq. (18). Top: comparison of ZR and BO results in the case $M = m$ for $c_{II} = 0$ (two lower curves) and $c_{II} = 0.2$ (two upper curves). Middle: impact of the mass ratio. Comparison of the BO results for $M = m$ (curves) and $M = 2m$ (curves with dots) at $c_{II} = 0$ and $c_{II} = 0.2$. Bottom: comparison of ZR and BO potentials for the mass ratio of a ${}^{133}\text{Cs}/{}^6\text{Li}$ mixture at $c_{II} = 0$ (two lower curves) and $c_{II} = 0.2$ (two upper curves).

V. SUMMARY/OUTLOOK

We investigate the problem of two bosonic impurities in a spin-polarized Fermi gas. First, we consider the ground state energy of the system in the Bethe-ansatz-solvable case, i.e., equal masses of fermions and impurities, $m = M$, as well as equal impurity-impurity and

impurity-fermion interactions, $c_{II} = c$. We calculate the ground state energy and show that there are attractive impurity-impurity interactions induced by the fermionic medium. In the next step, we discuss an effective model for the induced interactions and compare its predictions to the exact results. We use two effective potentials to define the effective Hamiltonian for the impurity system: a zero-range potential matched to single-phonon exchange and an adiabatic potential for heavy impurities derived in the Born-Oppenheimer approximation. Both potentials are able to reproduce the exact results from the Bethe-ansatz. The difference between the two model potentials for $m = M$ allows us to estimate the errors and the breakdown of our effective Hamiltonian. For the Bethe-ansatz-integrable case the difference between the results derived using the two effective potentials is marginal, which argues in favor of using them for qualitative analysis of Fermi gases with impurities.

The success of the effective model in the integrable case motivates our use of the effective model to study non-integrable systems characterized by relaxing at least one of the two conditions $m = M$ and $c_{II} = c$. For repulsive impurity-impurity interactions in free space, $c_{II} > 0$, we predict that the induced interaction overcomes the free space interaction and an in-medium bound state is formed if the impurity-fermion interaction satisfies $c < -\pi\sqrt{c_{II}}$. The binding energies are larger for heavier impurities such that the observation of in-medium bound states in heavy-light mixtures appears more promising.

Our findings show that the Bethe-ansatz-solvable models provide a playground for investigating induced interactions. In the future it will be interesting to use the Bethe ansatz equations (6) to investigate spatial correlations of two impurities, which will allow us to test an effective model beyond the simple energy comparison presented here. Further studies of non-integrable systems are also needed. The non-integrability due to $c_{II} \neq c$ and $m \neq M$ has been briefly discussed here. For cold atoms it is important also to consider trap effects, which break the integrability and change the properties of the system [58, 59].

It will be interesting to extend present study to fermionic impurities. It is known that two fermionic impurities in the SU(2) case do not have an in-medium bound state [60]. However, if the impurities are very heavy then a bound state must exist: The BO potential in Fig. 3 unlike the zero-range potential of Eq. (16) has a finite range, and hence supports a bound state as $M \rightarrow \infty$. This prediction can be explored using numerical many-body methods that are able to deal with mass-imbalanced systems such as the complex Langevin approach [61, 62].

ACKNOWLEDGMENTS

We thank Lukas Rammelmüller for useful discussions and comments on the manuscript. This work has

been supported by the Deutsche Forschungsgemeinschaft (DFG, German Research Foundation) under project numbers 413495248 – VO 2437/1-1 and 279384907 – SFB 1245 and by the Bundesministerium für Bildung und Forschung (BMBF) through contract 05P18RDFN1.

Appendix A: Weak coupling expansion

In this appendix, we derive a weak coupling expansion of the BA equations,

$$e^{ik_j l} = \frac{k_j - \Lambda_1 + \frac{ic}{2}}{k_j - \Lambda_1 - \frac{ic}{2}} \frac{k_j - \Lambda_2 + \frac{ic}{2}}{k_j - \Lambda_2 - \frac{ic}{2}}, \quad 1 \leq j \leq N; \quad (\text{A1})$$

$$\prod_{j=1}^N \frac{k_j - \Lambda_1 + \frac{ic}{2}}{k_j - \Lambda_1 - \frac{ic}{2}} = 1, \quad \prod_{j=1}^N \frac{k_j - \Lambda_2 + \frac{ic}{2}}{k_j - \Lambda_2 - \frac{ic}{2}} = 1, \quad (\text{A2})$$

where N is an odd number. First, we consider the wave vectors k_j ($j = 3, \dots, N$) that satisfy $k_j(c = 0) \neq 0$. For $c = 0$, these wave vectors are multiples of $2\pi/l$. When $c \neq 0$, we write them as

$$k_j = \frac{2\pi}{l} m_j + \delta_j, \quad m_j \in \mathbb{Z} \setminus \{0\}; \quad (\text{A3})$$

where δ_j is small. Inserting Eq. (A3) into the left-hand-side of Eq. (A1) leads to

$$e^{ik_j l} = \underbrace{e^{im_j 2\pi}}_{=1} e^{i\delta_j l} \approx 1 + i\delta_j l. \quad (\text{A4})$$

We write the right-hand-side of Eq. (A1) as

$$\frac{k_j - \Lambda_1 + \frac{ic}{2}}{k_j - \Lambda_1 - \frac{ic}{2}} \frac{k_j - \Lambda_2 + \frac{ic}{2}}{k_j - \Lambda_2 - \frac{ic}{2}} \approx 1 + \frac{2ic}{k_j^{(0)}}, \quad (\text{A5})$$

where terms proportional to c^n with $n > 1$ are neglected. Also it is assumed that $k_j^{(0)} \gg \delta_j - \Lambda_1$ and $k_j^{(0)} \gg \delta_j - \Lambda_2$. This assumption is valid, since the Λ 's lie in between the first three wave vectors, which are all close to zero. To derive Eq. (A5), we use that for $a \gg b$

$$\frac{a+b}{a-b} \approx 1 + \frac{2b}{a}. \quad (\text{A6})$$

With Eqs. (A4) and (A5), we obtain

$$\delta_j l = \frac{2c}{k_j^{(0)}} \Rightarrow \delta_j = \frac{c}{\pi m_j}. \quad (\text{A7})$$

Now we investigate the wave vectors k_j that vanish at $c = 0$. As discussed in the main text, for the ground state, $k_1 = -k_2$ and $k_3 = 0$. To show that $\Lambda_1 = -\Lambda_2$, we consider Eq. (A1) for k_1 and k_2 . We use $k_1 = -k_2$ in the equation for k_2 :

$$e^{-ik_1 l} = \frac{-k_1 - \Lambda_1 + \frac{ic}{2}}{-k_1 - \Lambda_1 - \frac{ic}{2}} \frac{-k_1 - \Lambda_2 + \frac{ic}{2}}{-k_1 - \Lambda_2 - \frac{ic}{2}} \quad (\text{A8})$$

$$\rightarrow e^{ik_1 l} = \frac{k_1 + \Lambda_1 + \frac{ic}{2}}{k_1 + \Lambda_1 - \frac{ic}{2}} \frac{k_1 + \Lambda_2 + \frac{ic}{2}}{k_1 + \Lambda_2 - \frac{ic}{2}}. \quad (\text{A9})$$

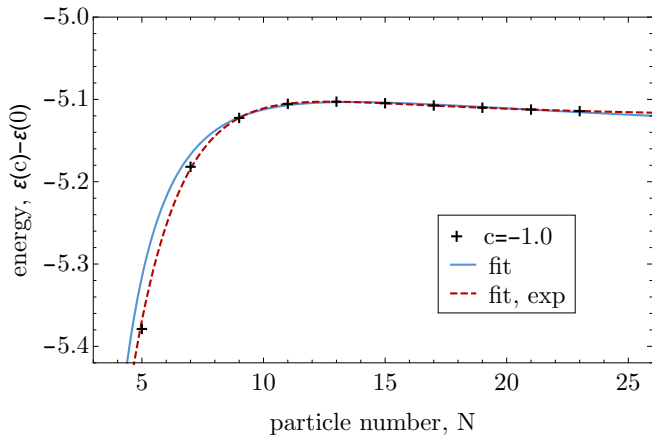


Figure 6. The energy $\varepsilon(c) - \varepsilon(0)$ as a function of the particle number N for $c = -1.0$. The (blue) solid line corresponds to the fit with Eq. (B1), in which case $\varepsilon_\infty = -5.176$. The (red) dashed curve shows the fit with Eq. (B2), leading to $\varepsilon_\infty = -5.125$.

From this equation and the equation for k_1 :

$$e^{ik_1 l} = \frac{k_1 - \Lambda_1 + \frac{ic}{2}}{k_1 - \Lambda_1 - \frac{ic}{2}} \frac{k_1 - \Lambda_2 + \frac{ic}{2}}{k_1 - \Lambda_2 - \frac{ic}{2}}, \quad (\text{A10})$$

we obtain that $\Lambda_1 = -\Lambda_2$. Using the equation for k_1 , we derive

$$1 + ik_1 l \approx 1 + \frac{2ick_1}{k_1^2 - \Lambda_1^2} \quad (\text{A11})$$

$$\Leftrightarrow (k_1^2 - \Lambda_1^2)l = 2c.$$

Next, we consider Eq. (A2). The sum of the wave vectors $\{k_3, \dots, k_N\}$ is zero, thus, Eq. (A2) can be rewritten as

$$\prod_{j=1}^3 \frac{k_j - \Lambda_1 + \frac{ic}{2}}{k_j - \Lambda_1 - \frac{ic}{2}} = 1. \quad (\text{A12})$$

With $k_1 = -k_2$, $k_3 = 0$, this equation reads

$$\frac{1}{k_1 - \Lambda_1} - \frac{1}{k_1 + \Lambda_1} - \frac{1}{\Lambda_1} = 0 \rightarrow \Lambda_1^2 = \frac{k_1^2}{3}. \quad (\text{A13})$$

We rewrite Eq. (A11)

$$(k_1^2 - \Lambda_1^2)l = \frac{2}{3}k_1^2 l = 2c, \quad (\text{A14})$$

which leads to $k_1 = \sqrt{3c/l}$ and $\Lambda_1 = \sqrt{c/l}$.

Appendix B: Thermodynamic extrapolation

To extrapolate the calculated energies $\varepsilon(c) - \varepsilon(0)$ to the thermodynamic limit, we shall employ the two fit

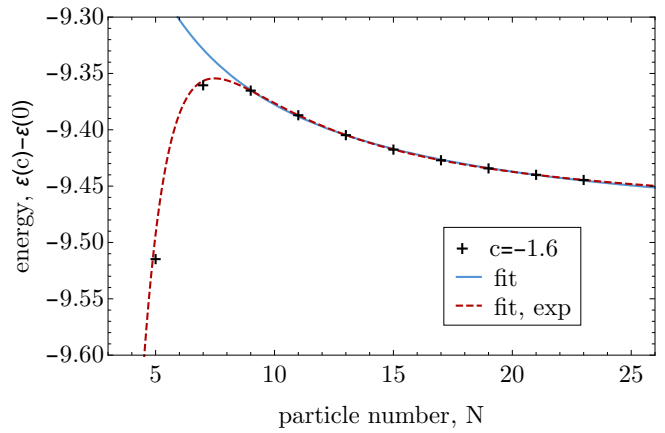


Figure 7. The energy $\varepsilon(c) - \varepsilon(0)$ as a function of the particle number N for $c = -1.6$. The (blue) solid line corresponds to the fit with Eq. (B1), in which case $\varepsilon_\infty = -9.499$. The (red) dashed curve shows the fit with Eq. (B2), leading to $\varepsilon_\infty = -9.479$.

functions:

$$1) \quad \varepsilon_\infty + \frac{A_1}{N} + \frac{A_2}{N^2}, \quad (\text{B1})$$

$$2) \quad \varepsilon_\infty + \frac{A_1}{N^\alpha} + A_2 e^{-\beta N}. \quad (\text{B2})$$

To illustrate the fits, we show in Figs. 6 and 7 the exact energies as functions of N for two different interaction strengths together with the corresponding fits. Both functions (B1) and (B1) appear to represent the data well. They also produce similar results for $N \rightarrow \infty$. The values of ε_∞ from the two fits differ only in the third digit, implying that the precise knowledge of the convergence pattern as $N \rightarrow \infty$ is not needed for the considered parameters.

Appendix C: One impurity

Here we briefly review how to derive the ground state energy of a Fermi gas with a single impurity atom. This system has already been investigated [36]. We use this well-known set-up to test our numerical approach. The system is described the Hamiltonian

$$h_{BA} = - \sum_{j=1}^N \frac{\partial^2}{\partial x_j^2} + 2c \sum_{j<l}^N \delta(x_j - x_l), \quad (\text{C1})$$

where the coordinates x_1, \dots, x_{N-1} are the positions of the fermions, and x_N is reserved for the impurity. The

corresponding Bethe ansatz equations are given by [32]

$$e^{ik_j^{(1)}l} = \frac{k_j^{(1)} - \Lambda + \frac{1}{2}ic}{k_j^{(1)} - \Lambda - \frac{1}{2}ic}, \quad 1 \leq j \leq N; \quad (\text{C2})$$

$$\prod_{j=1}^N \frac{k_j^{(1)} - \Lambda + \frac{1}{2}ic}{k_j^{(1)} - \Lambda - \frac{1}{2}ic} = 1,$$

where $k_j^{(1)}$ is the j th wave vector (we use the superscript to emphasize that we work with a single impurity here), and Λ is one additional variable. We consider N to be even. Once the BA equations are solved, the energy can be calculated as $\varepsilon^{(1)} = \sum_j \left(k_j^{(1)}\right)^2$.

We solve the BA equations with Newton's method as already explained in the main part. For small c the weak coupling expansion of the BA equations [63] is used as an initial guess

$$k_1^{(1)} \approx -\frac{1}{4\pi} \sum_{j=3}^N \frac{1}{m_j} c + \sqrt{\frac{c}{l}},$$

$$k_2^{(1)} \approx -\frac{1}{4\pi} \sum_{j=3}^N \frac{1}{m_j} c - \sqrt{\frac{c}{l}}, \quad (\text{C3})$$

$$k_j^{(1)} \approx \frac{2\pi}{l} m_j + \frac{1}{2\pi m_j} c \quad \text{for } 3 \leq j \leq N; \Lambda \approx \gamma c,$$

where $m_j \in \mathbb{Z}$ determine the wave vectors of the particles for zero interaction. The shift due to the small interaction is given by the terms proportional to c and \sqrt{c} .

To extrapolate the result to the thermodynamic limit we use $\varepsilon^{(1)}(c) - \varepsilon^{(1)}(0) = \mathcal{E} + \alpha/N^\beta$, where \mathcal{E} , α and β are fit parameters. We show the result in Fig. 8. Our result fits the analytic expression quite well. The relative difference, shown in the inset, is negligible for our purposes. We present also the result for 14 particles to demonstrate that only a handful of particles are needed to simulate the ground state properties of an infinite Fermi gas with an impurity in a laboratory.

Appendix D: Two static impurities

Here we calculate the eigenenergies of the Hamiltonian

$$h_{BO} = -\frac{\partial^2}{\partial x^2} + 2c \left[\delta\left(x - \frac{r}{2}\right) + \delta\left(x + \frac{r}{2}\right) \right]. \quad (\text{D1})$$

To this end, we divide the space into three parts: $-l/2 < x < -r/2$, $-r/2 < x < r/2$, and $r/2 < x < l/2$. For each part we write the wave function as

$$\psi(x) = a_1 e^{ikx} + a_2 e^{-ikx}, \quad (\text{D2})$$

where k is the wave number. The wave function must obey the ‘‘delta-potential boundary conditions’’ at $x = \pm r/2$, and periodic boundary conditions at $x = \pm l$. We divide the solutions into parity-symmetric and parity-antisymmetric ones. Furthermore, we consider ‘‘bound states’’ and ‘‘scattering states’’ separately. For ‘‘bound

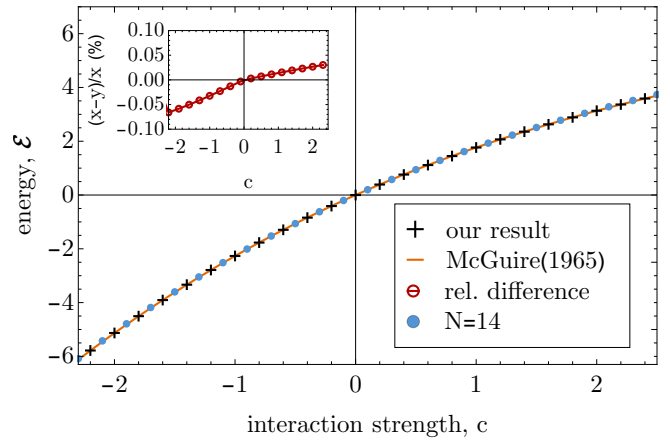


Figure 8. The energy of an impurity atom in a Fermi gas, \mathcal{E} , as a function of the interaction strength, c . The crosses represent our numerical result for the thermodynamic limit. The analytic result for the thermodynamic limit [36] is shown by the orange line. In addition the total energy for a system consisting of $N = 14$ particles is shown by the blue dots. Inset: The red circles display the relative difference $(x-y)/x$, where x is our numeric result and y the analytic expression from Ref. [36]. The curve is added to guide the eye.

states’’ the wave vector is imaginary, so the ansatz $k = i\kappa$ is made, where κ is real. For ‘‘scattering states’’, the wave vector is real. The equations that determine k for each class of solutions are written below.

1) Symmetric ‘‘bound states’’:

$$-2\kappa e^{\frac{\kappa l}{2} + \kappa r} (2ce^{-\kappa l} + ge^{-\kappa l - \kappa r} + 2ce^{-\kappa r} + 2ce^{-2\kappa r} - 2\kappa e^{-\kappa l - \kappa r} + 2\kappa e^{-\kappa r}) = 0. \quad (\text{D3})$$

2) Antisymmetric ‘‘bound states’’:

$$2e^{\frac{\kappa l}{2} + \kappa r} (2ce^{-\kappa l} - 2ce^{-\kappa l - \kappa r} - 2ce^{-\kappa r} + 2ce^{-2\kappa r} + 2\kappa e^{-\kappa l - \kappa r} - 2\kappa e^{-\kappa r}) = 0. \quad (\text{D4})$$

3) Symmetric ‘‘scattering states’’:

$$k \left[2c \left(\cos\left(\frac{kl}{2}\right) + \cos\left(\frac{1}{2}k(l-2r)\right) \right) - 2k \sin\left(\frac{kl}{2}\right) \right] = 0. \quad (\text{D5})$$

4) Antisymmetric ‘‘scattering states’’:

$$8c \cos\left(\frac{1}{2}k(l-2r)\right) - 8c \cos\left(\frac{kl}{2}\right) \quad (\text{D6})$$

$$+ 8k \sin\left(\frac{kl}{2}\right) = 0. \quad (\text{D7})$$

To solve the equations, a genetic algorithm first finds approximate solutions for k, κ . These are then used in the Newton's iteration method as an initial guess. We calculate as many energy levels as particles we consider.

- [1] L. D. Landau and S. I. Pekar, *J. Exp. Theor. Phys* **18**, 419 (1948).
- [2] S. Pekar., Research in Electron Theory of Crystals (AEC-tr-555, US Atomic Energy Commission, 1963).
- [3] A. S. Alexandrov and N. F. Mott, Polarons and Bipolarons (World Scientific, Singapore, 1995).
- [4] G. Baym and C. Pethick, Landau Fermi-Liquid Theory: Concepts and Applications (2008).
- [5] M. Kutschera and W. Wójcik, *Phys. Rev. C* **47**, 1077 (1993).
- [6] A. Schirotzek, C.-H. Wu, A. Sommer, and M. W. Zwierlein, *Phys. Rev. Lett.* **102**, 230402 (2009).
- [7] S. Nascimbène, N. Navon, K. J. Jiang, L. Tarruell, M. Teichmann, J. McKeever, F. Chevy, and C. Salomon, *Phys. Rev. Lett.* **103**, 170402 (2009).
- [8] P. Massignan, M. Zaccanti, and G. M. Bruun, *Rep. Prog. Phys.* **77**, 034401 (2014).
- [9] M.-G. Hu, M. J. Van de Graaff, D. Kedar, J. P. Corson, E. A. Cornell, and D. S. Jin, *Phys. Rev. Lett.* **117**, 055301 (2016).
- [10] N. B. Jørgensen, L. Wacker, K. T. Skalmstang, M. M. Parish, J. Levinsen, R. S. Christensen, G. M. Bruun, and J. J. Arlt, *Phys. Rev. Lett.* **117**, 055302 (2016).
- [11] R. Schmidt, M. Knap, D. A. Ivanov, J.-S. You, M. Cetina, and E. Demler, *Rep. Prog. Phys.* **81**, 024401 (2018).
- [12] M. Bruderer, A. Klein, S. R. Clark, and D. Jaksch, *Phys. Rev. A* **76**, 011605 (2007).
- [13] M. Schechter and A. Kamenev, *Phys. Rev. Lett.* **112**, 155301 (2014).
- [14] K. Keiler, S. Krönke, and P. Schmelcher, *New Journal of Physics* **20**, 033030 (2018).
- [15] P. Naidon, *Journal of the Physical Society of Japan* **87**, 043002 (2018).
- [16] A. S. Dehkharghani, A. G. Volosniev, and N. T. Zinner, *Phys. Rev. Lett.* **121**, 080405 (2018).
- [17] A. Camacho-Guardian and G. M. Bruun, *Phys. Rev. X* **8**, 031042 (2018).
- [18] A. Camacho-Guardian, L. A. Peña Ardila, T. Pohl, and G. M. Bruun, *Phys. Rev. Lett.* **121**, 013401 (2018).
- [19] A. I. Pavlov, J. van den Brink, and D. V. Efremov, *Phys. Rev. B* **98**, 161410 (2018).
- [20] S. Mistakidis, G. Katsimiga, G. Koutentakis, and P. Schmelcher, *New Journal of Physics* **21**, 043032 (2019).
- [21] B. Reichert, Z. Ristivojevic, and A. Petkovic, *New Journal of Physics* **21**, 053024 (2019).
- [22] B. J. DeSalvo, K. Patel, G. Cai, and C. Chin, *Nature* **568**, 61 (2019).
- [23] A. Alexandrov and N. F. Mott, *Rep. Prog. Phys.* **57**, 1197 (1994).
- [24] Experiments with ultracold atoms can give important insight into the physics of induced attractive potentials. However, atoms interact via short-range potentials and cannot simulate all properties of bound states of dressed electrons. For example, the predicted abrupt change of the mean distance between two polarons across the unbound-polarons to bipolaron transition [55] most probably cannot be simulated in these experiments because the Coulomb interaction is an important ingredient for observing this effect [64].
- [25] Y. Takada, *Phys. Rev. B* **26**, 1223 (1982).
- [26] Note that any attractive potential supports at least one bound state in the 1D world [38].
- [27] J. Friedel, *Il Nuovo Cimento* (1955-1965) **7**, 287 (1958).
- [28] M. A. Cazalilla, R. Citro, T. Giamarchi, E. Orignac, and M. Rigol, *Rev. Mod. Phys.* **83**, 1405 (2011).
- [29] X.-W. Guan, M. T. Batchelor, and C. Lee, *Rev. Mod. Phys.* **85**, 1633 (2013).
- [30] M. T. Batchelor and A. Foerster, *Journal of Physics A: Mathematical and Theoretical* **49**, 173001 (2016).
- [31] G. Pagano, M. Mancini, G. Cappellini, P. Lombardi, F. Schäfer, H. Hu, X.-J. Liu, J. Catani, C. Sias, M. Inguscio, and L. Fallani, *Nature Physics* **10**, 198 (2014).
- [32] C. N. Yang, *Phys. Rev. Lett.* **19**, 1312 (1967).
- [33] C. K. Lai and C. N. Yang, *Phys. Rev. A* **3**, 393 (1971).
- [34] M. T. Batchelor, M. Bortz, X. W. Guan, and N. Oelkers, *Phys. Rev. A* **72**, 061603 (2005).
- [35] A. Imambekov and E. Demler, *Phys. Rev. A* **73**, 021602 (2006).
- [36] J. B. McGuire, *Journal of Mathematical Physics* **6**, 432 (1965).
- [37] J. B. McGuire, *Journal of Mathematical Physics* **7**, 123 (1966).
- [38] L. D. Landau and E. M. Lifschitz, Quantum Mechanics: Non-relativistic Theory (3rd edition) (Elsevier Butterworth-Heinemann, 1977).
- [39] B. Simon, *Ann. Phys.* **97**, 279 (1976).
- [40] A. G. Volosniev, D. V. Fedorov, A. S. Jensen, M. Valiente, and N. T. Zinner, *Nature Communications* **5**, 5300 (2014).
- [41] F. Deuretzbacher, D. Becker, J. Bjerlin, S. M. Reimann, and L. Santos, *Phys. Rev. A* **90**, 013611 (2014).
- [42] A. G. Volosniev, D. Petrosyan, M. Valiente, D. V. Fedorov, A. S. Jensen, and N. T. Zinner, *Phys. Rev. A* **91**, 023620 (2015).
- [43] P. Massignan, J. Levinsen, and M. M. Parish, *Phys. Rev. Lett.* **115**, 247202 (2015).
- [44] F. Deuretzbacher, D. Becker, J. Bjerlin, S. M. Reimann, and L. Santos, *Phys. Rev. A* **95**, 043630 (2017).
- [45] A. G. Volosniev, *Few-Body Systems* **58**, 54 (2017).
- [46] R. P. Hodgson and J. B. Parkinson, *Journal of Physics C: Solid State Physics* **17**, 3223 (1984).
- [47] A. Recati, J. N. Fuchs, C. S. Peça, and W. Zwerger, *Phys. Rev. A* **72**, 023616 (2005).
- [48] J. N. Fuchs, A. Recati, and W. Zwerger, *Phys. Rev. A* **75**, 043615 (2007).
- [49] L. Parisi and S. Giorgini, *Phys. Rev. A* **95**, 023619 (2017).
- [50] P. W. Anderson, *Phys. Rev. Lett.* **18**, 1049 (1967).
- [51] H. Castella and X. Zotos, *Phys. Rev. B* **47**, 16186 (1993).
- [52] S. Giraud and R. Combescot, *Phys. Rev. A* **79**, 043615 (2009).
- [53] R. Mao, X. W. Guan, and B. Wu, *Phys. Rev. A* **94**, 043645 (2016).
- [54] A. G. Volosniev and H.-W. Hammer, *New Journal of Physics* **19**, 113051 (2017).
- [55] J. Adamowski, *Phys. Rev. B* **39**, 3649 (1989).
- [56] P. Vansant, M. A. Smondyrev, F. M. Peeters, and J. T. Devreese, *Journal of Physics A: Mathematical and General* **27**, 7925 (1994).
- [57] For strong interactions, this case can still be studied with integrable Heisenberg Hamiltonians using the mapping

onto a spin chain [40–43]. We do not discuss this limit here, instead we focus on the regimes with weak and moderate interactions.

- [58] N. T. Zinner, EPJ Web of Conferences **113**, 01002 (2016).
- [59] T. Sowiński and M. Á. García-March, [arXiv:1903.12189](#).
- [60] M. Flicker and E. H. Lieb, Phys. Rev. **161**, 179 (1967).
- [61] L. Rammelmüller, W. J. Porter, J. E. Drut, and J. Braun, Phys. Rev. D **96**, 094506 (2017).
- [62] L. Rammelmüller, J. E. Drut, and J. Braun, Journal of Physics: Conference Series **1041**, 012006 (2018).
- [63] N. Oelkers, M. T. Batchelor, M. Bortz, and X.-W. Guan, Journal of Physics A: Mathematical and General **39**, 1073 (2006).
- [64] C. H. Schmickler, H. W. Hammer, and A. G. Volosniev, [arXiv:1904.00913](#).